6th AIAA Flow Control Conference
25 - 28 June 2012, New Orleans, Louisiana

AIAA 2012-3052

Unsteady Forcing of a Post-stall Flow Over a NACA0012 Airfoil by a Surface DBD Actuator

Audier P.,* and Hong D.†

GREMI, UMR 7344 CNRS/University of Orléans, 14 rue d'Issoudun, 45067 Orléans Cedex 2, France

Leroy A.‡

PRISME, University of Orléans, 8 rue Léonard de Vinci, 45072 Orléans Cedex 2, France

The present study deals with the enhancement of a NACA0012 aerodynamic airfoil performance by using a thin DBD actuator to control flow separation occurring around the leading-edge. The post-stall separated flow over an airfoil is characterized at least by a shear layer emitted from the leading edge that corresponds to convective process instability and a wake flow corresponding to a global instability behavior, related to a vortex shedding. According to the forcing frequencies, different modifications of the shear layer rollup and wake vortex shedding can usually be observed. This study highlights the actuator effects by unsteady actuation with forcing frequencies selected according to the natural frequency of the wake vortex shedding. Mean aerodynamic force measurements, PIV and hot-wire anemometry in the vicinity of the shear layer and in the far wake were performed to characterize the benefits of the control. For a deep post-stall airflow, results show that forcing frequencies closer to the wake vortex shedding frequency lead to achieve a high increase in lift.

Nomenclature

α	Incidence, degree
C	Chord, m
CD	Drag coefficient with actuation
CD_{off}	Drag coefficient without actuation
CL	Lift coefficient with actuation
CL_{off}	Lift coefficient without actuation
F^+	Reduced frequency
F_{burst}	Burst frequency, Hz
F_{HV}	High voltage frequency, Hz
F_{nat}	Natural frequency measured next to the shear layer, Hz
F_{wake}	Wake shedding vortices frequency, Hz
St	Strouhal number
U_∞	Free stream velocity, m.s^{-1}
U_{mean}	Mean value of the wall-normal velocity, m.s^{-1}
U_{RMS}	Root mean square value of the wall-normal velocity, m.s^{-1}
V_{HV}	High voltage amplitude, kV

*PhD Student, University of Orléans, GREMI, 14 rue d'Issoudun 45067 Orléans Cedex 2 France
†Professor, University of Orléans, GREMI, 14 rue d'Issoudun 45067 Orléans Cedex 2 France
‡Associate Professor, University of Orléans, PRISME, 8 rue Léonard de Vinci, 45072 Orléans Cedex 2 France

I. Introduction

ACTIVE flow control by plasma actuators is currently studied in order to control external flows on aerodynamic geometries. Past studies[1–3] give an overview of various configurations based on the surface Dielectric Barrier Discharge (DBD) and highlight the ability of this type of actuators to manipulate flows. Actual limitation of the ionic wind magnitude obtained from DBD actuators lead to optimize actuator authority to investigate flow control by unsteady actuation rather than steady actuation. In unsteady actuation, a key control parameter is the burst frequency which periodically imposes switching on and off the actuator.

The post-stall separated flow over an airfoil is characterized at least by a shear layer emitted from the leading edge that corresponds to convective process instability (Kelvin-Helmholtz type instability) and a wake flow corresponding to a global instability behavior, related to a large scale vortex shedding. This suggests that there is more than one natural time scale in a post-stall regime. Consequently both instabilities are important to control the separated flow by unsteady actuation. Depending on the kind of actuation and the flow regime considered, a large range of effective forcing frequencies are reported in the literature via numerical and experimental studies. Several past studies[4–10] have shown that F^+, the reduced frequency of excitation based on the chord length and the freestream velocity, roughly equal to unity, provides aerodynamic performance enhancement. In general, what it is sought is to affect instabilities of the separating shear layer in order to exploit a coanda-like deflection of this latter towards the airfoil suction side. For post-stall regime, Wu et al[11] argued it was reasonable to assume these two above simple flow features interact according to a nonlinear process and then it is possible to perform a control of the massively separated flow, with low-level power input near the leading-edge, by periodic excitation scaled on the wake flow instability or its harmonics. Following this assumption, Ref.[12–14] have reported lift increase by different kind of control devices. This experimental study attempts to explore capabilities of a sine DBD actuator, being operated near the leading edge with a low power input, to improve aerodynamic performance in stall regime by focusing on periodic excitation scaled on the wake flow instability. The main objectives are to find out the most effective burst frequency and to exhibit the corresponding physical mechanism responsible for this.

The results presented in this paper were obtained for a NACA 0012 airfoil at a high incidence in a freestream flow of $20\,\mathrm{m.s^{-1}}$, equipped with a single thin DBD actuator located at its leading edge. To examine the flow physics associated with stall and its response to the forcing frequency, aerodynamic force measurements, Particle Imaging Velocimetry (PIV) and hot-wire anemometry measurements have been performed to characterize the uncontrolled and controlled flow and the control benefits.

II. Experimental set-up

A. Airfoil and actuator

These experiments have been conducted at the University of Orléans, in the Lucien Malavard close return wind tunnel. The test section is 5 m long with a cross-section of 2 m x 2 m. The operating speed of the wind tunnel varies from $10\,\mathrm{m.s^{-1}}$ to $60\,\mathrm{m.s^{-1}}$ with an airflow turbulence level below 0.4%. A plexiglas window mounted on one side enables the PIV measurements. The airfoil used in this study was a NACA0012 profile with a chord dimension of C=0.3 m and a span wise length of 1.1 m. It was mounted between two flat planes in order to achieve a 2D flow configuration (Fig.1). The wing was mounted on both tips to a 6 component platform balance used for time-averaged lift and drag measurements and located under the test section. Experiments described in this paper have been carried out for a velocity of U_∞=$20\,\mathrm{m.s^{-1}}$, resulting in a Reynolds number based on the airfoil chord length of 400 000.

The actuator consisted of two copper electrodes flush mounted with an asymmetric disposition on both sides of a dielectric sheet constituted by four layers of Kapton©, representing a total thickness of 0.5 mm. The active air-exposed electrode of the plasma actuator was placed at the leading edge of the airfoil as described in Fig.2. The grounded electrode was encapsulated in order to create discharges only on the upper side of the dielectric sheet which was exposed to the ambient air. The 6 mm wide and 1 m long electrodes were separated by a gap of 3mm and connected to an AC high voltage power supply. The electrodes had a large dimension (90% of the span wise length) in order to maximize the plasma actuation on the airfoil and to keep a 2D flow configuration as much as possible. The plasma was obtained with a steady or unsteady actuation performed by applying a sinusoidal signal to the air-exposed electrode with a high-voltage amplitude V_{HV}=8 kV and a frequency F_{HV}=2 kHz. For the unsteady actuation, the burst frequency varied up to 500 Hz and the duty

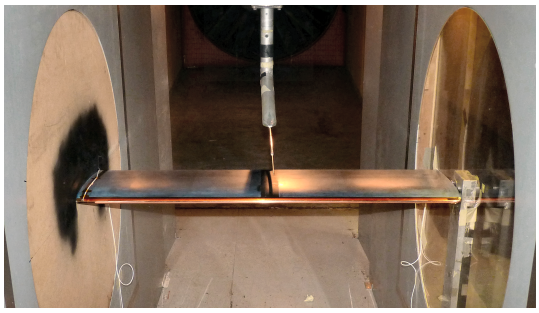

Figure 1. NACA0012 airfoil in the test section.

cycle was fixed to 50%. The ionic wind velocity produced by the actuator was approximately of $3\,\mathrm{m.s^{-1}}$ and acts as a thin wall jet, as shown in a previous paper[15]. The active power dissipated was estimated at $15\,\mathrm{W.m^{-1}}$ roughly according to a common calculation method[16].

B. Measurements for aerodynamic flow investigation

Mean loads measurements were performed by the aerodynamic balance located under the main test section. The balance was carefully calibrated and lift and drag coefficient uncertainties were estimated to be less than 2%.

Measurements of temporal flow velocities were made using two single hot-wire probes (Dantec Dynamics, 55P11). The probes were calibrated from 1 to $45\,\mathrm{m.s^{-1}}$ using a Dantec calibration unit. The two hot-wire signals were simultaneously processed and recorded via the Dantec Constant-Temperature-Anemometer (Streamline 90N10 Frame). One single hot wire probe was mounted on the moving 3-axis traversing system installed above the test section and was used to perform velocity measurements in the vicinity of the shear layer. The other one was mounted on a system fixed on the floor of the test section near the wake as shown in Fig.2. Each velocity measurement consisted of the average of 524288 samples. The acquisition frequency was set to 6 kHz and signals are low-pass filtered at 3 kHz. The sampling rate is high enough to use temporal flow velocity series to calculate Power Spectra Density (PSD).

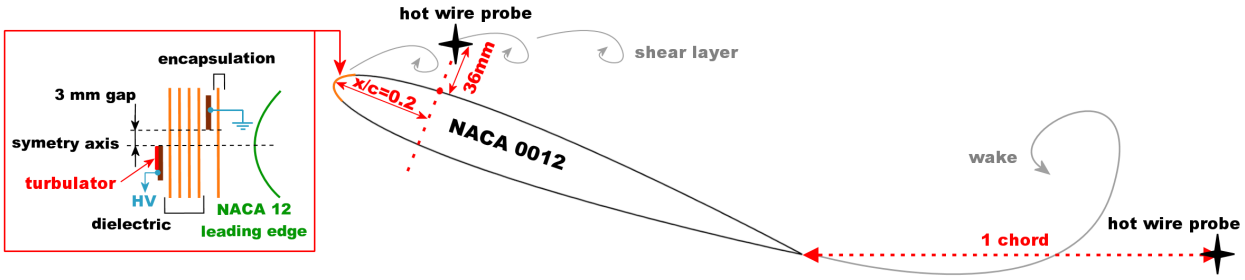

Figure 2. Location of hot-wire probes around the NACA0012 and structure of the actuator.

Mean velocity fields and mean velocity fluctuations around the airfoil were studied from 2D-PIV measurements in order to choose the position of the hot-wire probes and to analyze flow separation features in the symmetry longitudinal plane. PIV system consisted of a double pulsed Nd:Yag laser emitting pulses of 200 mJ. The laser light sheet was placed parallel to the streamwise direction in the median plane. Images were acquired with two TSI Power View Plus 2048 x 2048 pixels cameras fitted with a 105 mm lens to covered the whole separation region around the airfoil. The image size was 431 mm x 248 mm with a spatial resolution of 122 μm per pixels. The seeding consisted of submicrosized olive oil droplets sprayed by a PIVTEC seeding system. For this configuration 1000 image pairs were recorded to ensure good statistics.

III. Results and discussions

A. Baseline uncontrolled flow

In this section are presented data from load measurements and hot wire measurements to characterize the baseline uncontrolled airflow, the actuator being implemented at the leading edge. Considering possible Reynolds effects at this free stream velocity, in order to investigate a case more corresponding to a turbulent boundary layer separation, 3D turbulators were used and located just ahead the actuator as shown in Fig.2. Lift coefficient versus incidence is plotted in Fig.3 for the separation of the natural and the tripped boundary layer, indicated by NBL and TBL respectively. It can be noted the TBL case curve can be assumed to represent flow separation of a turbulent boundary layer case because of the progressive lift loss after the stall incidence of 12°.

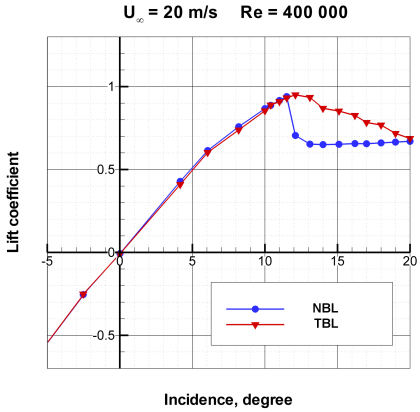

Figure 3. Lift coefficient versus incidence in natural (NBL) and tripped (TBL) boundary layer.

Fig.4 shows PSD of the fluctuating streamwise velocity at 20° of incidence, corresponding to a deep post stall regime. The position of the two probes is detailed in Fig.2. Results for the uncontrolled flow show the presence of two natural frequencies. The first one is indicated by PSD versus F^+ (F^+=F_{nat}.C/U_∞) plotted in the shear layer and corresponds to instabilities in the shear layer due to the separated boundary layer. The frequency bump is centered around F^+=3 in NBL and around F^+=5 in TBL. The second one is observable in PSD versus Strouhal number plotted in the wake region. As the airfoil is in deep stall, the bluff body wake shedding of vortices is characterized by the dominant Strouhal number (St=F_{wake}.C.sin(α)/U_∞) of about 0.2, commonly reported in the literature.

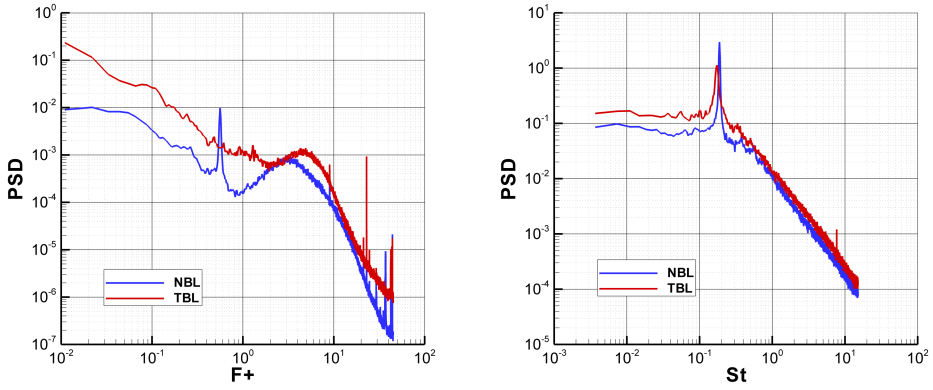

(a) Next to the shear layer

(b) In the wake

Figure 4. PSD of the fluctuating streamwise velocity, at a freestream flow of 20m.s^{-1} and 20° of incidence.

B. Burst modulation effects on mean aerodynamic loads

Time-averaged lift and drag coefficient gains for the controlled flow are presented in Fig.5 as a function of the burst frequency at 20° of incidence. The gain is defined by the ratios (CL - CL_{off})/CL_{off} and (CD - CD_{off})/CD_{off}. CL, CD, CL_{off} and CD_{off} correspond respectively to the aerodynamic coefficients for the controlled and the uncontrolled flow. These results show that the control is more efficient by unsteady actuation than in steady actuation in terms of lift coefficient gain. It also clearly indicates a frequency range at which lift gain is dramatic, namely around the low frequencies in the range of 30-40 Hz. This effective burst frequency matches with the wake frequency (St=0.2) observable in PSD plotted in the wake region in the first section. The Tab.1 summarizes lift and drag gains for the burst frequency of 35 Hz. It can be noted, even if drag is increased, lift to drag ratio gain remains positive because of the dramatic lift enhancement.

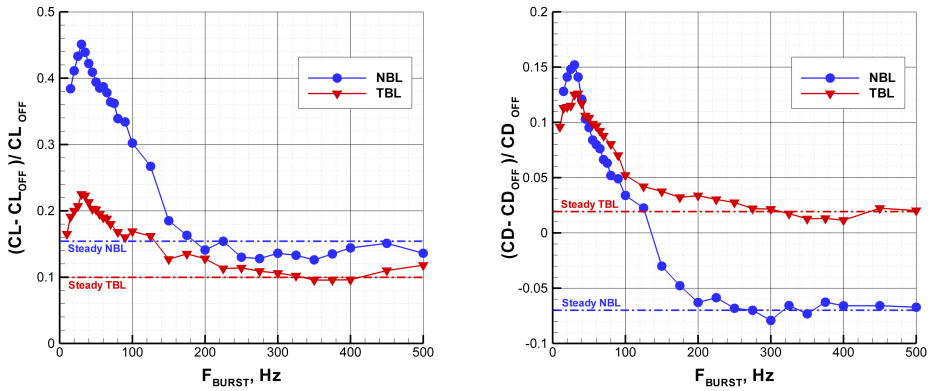

(a) Gain in Lift (b) Gain in Drag

Figure 5. Unsteady actuation - Lift and Drag coefficient gain versus F_{burst}. 20° of incidence.

Table 1. Gain values at the burst frequency of 35 Hz.

NBL	TBL
Lift increase of 45%	Lift increase of 20%
Drag increase of 15%	Drag increase of 10%
26% gain of CL/CD	9% gain of CL/CD

Considering natural or tripped boundary layer, results seem to exhibit the same range of effective forcing frequencies, but with the same power input, the control is more efficient in the NBL. Mechanisms involved in increasing lift must be finely investigated, because for this Reynolds number, a probable interaction of the actuator on the boundary layer nature and transition has to be considered as well. As it is difficult to estimate contribution of Reynolds effects, and, due to limitations of data measurement performed in this study, a focus on the dynamics of airflow is exclusively presented for the TBL case in the following section.

C. Burst modulation effects on the dynamics of airflow

In this section, results of flow investigation conducted to gain insight into actuation effects on the flow dynamics are presented for the following cases: non-controlled flow, flow controlled with a steady actuation, flow controlled with unsteady actuation. Two burst frequencies are selected according to previous results, namely 35 Hz (St=0.2), corresponding to the dominant wake frequency, and 350 Hz (F^+=5), further corresponding to the frequency bump of the shear layer.

1. Time averaged velocity fields on the suction side airfoil

Mean streamlines and flow velocity fields are plotted in Fig.6 at 20° of incidence in TBL.

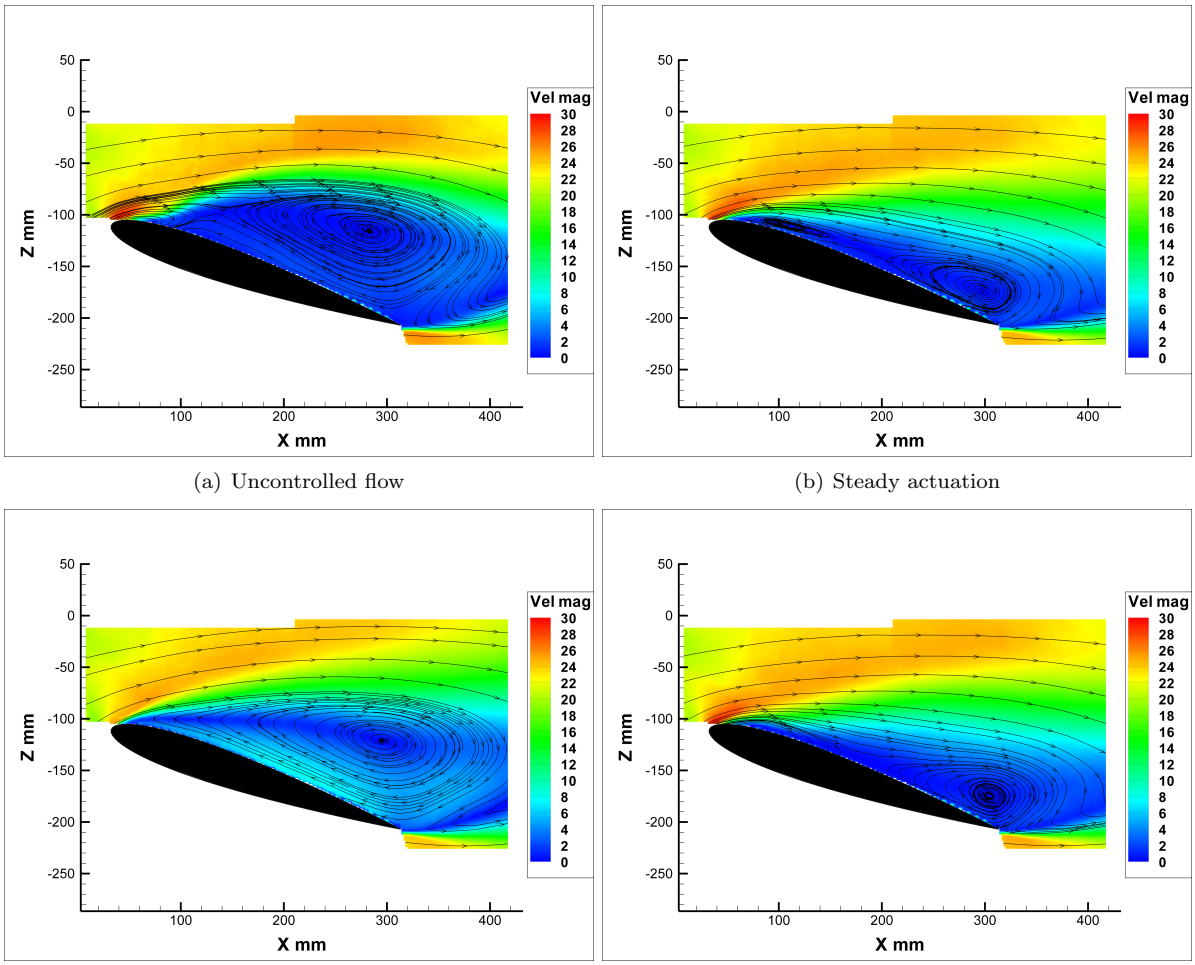

(a) Uncontrolled flow

(b) Steady actuation

(c) Unsteady actuation with F_{burst}=35 Hz

(d) Unsteady actuation with F_{burst}=350 Hz

Figure 6. Mean velocity contours and streamlines obtained by PIV at 20° of incidence.

It can be noted that the physical mechanisms involved in the enhancement of lift coefficient are different with steady or unsteady actuation. However no significant differences in flow separation topology were obtained with steady actuation and unsteady actuation at 350 Hz. The flow is not reattached over the airfoil for F_{burst}=35 Hz and from the streamlines, it can be observed a strong and large vortex established above the suction side extending from the leading edge to the trailing edge. As discussed in Ref.11, it is a strong lifting vortex, causing a flow field modification favorable to a large increase in lift. The physical mechanism involving this strong lifting vortex has been also observed for the NBL case for F_{burst}=35 Hz, but results are not presented here. In contrast, when forcing was provided at burst frequencies around 350 Hz or with steady actuation, a deflection of the shear layer toward the surface leading to a slight reduction of the separation bubble can be observed.

2. PSD of the fluctuating streamwise velocity component in the shear layer and wake regions

Influences of the burst frequencies on PSD of the fluctuating streamwise velocity component U_{RMS} are presented in Fig.7 in the shear layer and wake regions, for the uncontrolled flow, for the flow controlled by steady actuation and unsteady actuation (F_{burst}=35 Hz or 350 Hz). PSD were deduced from hot wire measurements performed at the positions indicated in Fig.2.

According to the burst frequency, shear layer and wake PSD show different actions of the unsteady forcing on the shear layer and wake natural instabilities. PSD of the unsteady forced flow in the shear layer exhibit strong peaks at the excitation frequency and its harmonics and show control process actually contributes to the production of some turbulence over a broad range of scales. The shear layer frequency bump is slightly

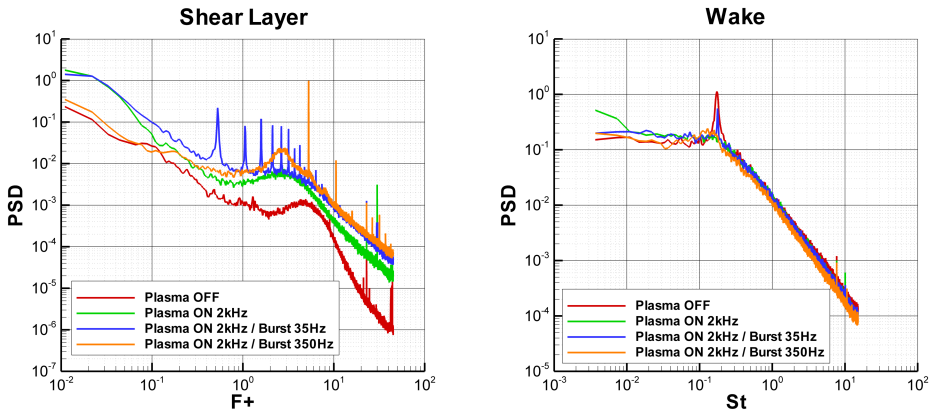

(a) Shear layer (b) wake

Figure 7. Shear layer and wake PSD for uncontrolled flow, controlled flow by steady actuation and unsteady actuation with F_{burst}=35 Hz and 350 Hz.

shifted towards lower frequencies for the three cases of controlled flow. PSD in the wake shows a strong peak relative to the wake vortex shedding only for the uncontrolled flow and the controlled flow at F_{burst}=35 Hz. That suggests an enhancement of the shear layer vortex rollup and diffusion while the unfavorable bluff body wake shedding of vortices might be disorganized, more particularly for the steady actuation and unsteady actuation at 350 Hz. At 35 Hz, the wake vortex shedding locks on the burst frequency. This can explain the drag increase for unsteady actuation at 35 Hz is more important than the ones measured for steady actuation and unsteady actuation at 350 Hz.

PSD in the wake region is shown in Fig.8 according to burst frequencies selected corresponding to a Strouhal number of 0.2. It has to be noted that the wake vortex shedding frequency locks on F_{burst}. This was not observed around higher forcing frequencies. This result highlights interaction and resonance between shear layer and wake vortex shedding as presented in Ref.11 and could be interesting in regard to closed loop control.

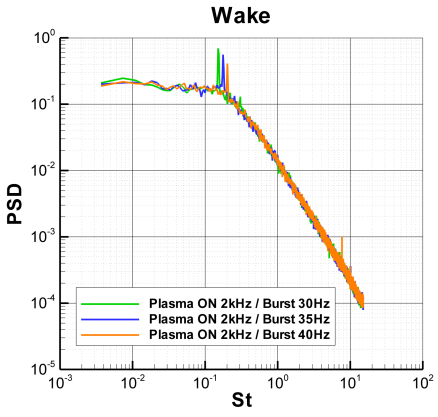

Figure 8. Wake PSD for controlled flow at F_{burst}=30 Hz, 35 Hz and 40 Hz.

3. Wake survey

To gain insight into actuation effects on the wake, mean streamwise velocity and its fluctuation profiles are plotted in Fig.9, for the uncontrolled flow and for the flow controlled by steady actuation and unsteady actuation (F_{burst}=35 Hz or 350 Hz).

Figure 9 clearly shows that the wake thickness and turbulence levels measured for the controlled case with

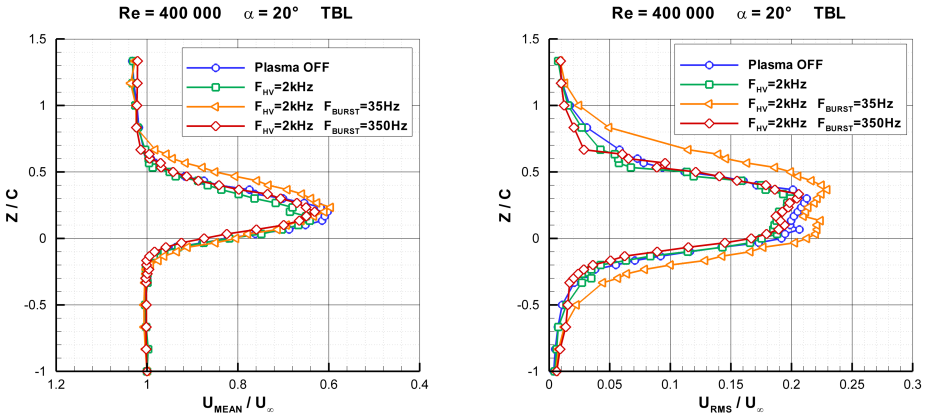

(a) U_{mean}/U_∞ (b) U_{RMS}/U_∞

Figure 9. Wake surveys at one chord downstream the trailing edge.

unsteady actuation at 35 Hz are larger than the others. This observation corroborates that drag increase, for unsteady actuation at 35 Hz, is more important than the ones measured for steady actuation and unsteady actuation at 350 Hz. For these latter cases, it was previously deduced from results a slight reduction of the separation bubble and an attenuation of the unfavorable bluff body wake shedding.

IV. Conclusion

The present study deals with the analysis of the effects of a controlled flow by a sine DBD actuator over a NACA 0012 airfoil at 20° of incidence and for a Reynolds number based on the airfoil chord length of 400000. It demonstrates that plasma local unsteady actuation, achieved with a quite low level power input and with an efficient forcing frequency matching the time-scale of the vortex shedding in the wake, can enable manipulation of the full separated flow in deep stall regime, leading to a lift increase. As it was reported in Ref.11, investigation of aerodynamic flow features suggest that excitation in the shear layer leads to the formation of a number of small vortices which merge to form a strong well-developed vortex larger than the separation vortex seen in the uncontrolled flow. The shear layer seems to extend in a direction tangent to the direction of separation. An interaction exists between the modified shear layer and vortices emitted in the wake because the wake vortex shedding locks on the forcing frequency. This flow field modification is favorable to a large increase in lift. In perspective, new study should be performed with time-resolved PIV to further analyse the mechanism of interaction between shear layer and wake. A parametric study about power input, which could be another key control parameter, should be done as well.

Acknowledgments

The research leading to these results has received funding from the European Community's Seventh Framework Program FP7/2007-2013 under grant agreement n°234201. The authors would like to thank S. Loyer for his technical support with the experimental set-up.

References

[1]Moreau, E., "Airflow control by non-thermal plasma actuators," *Journal of Physics D: Applied Physics*, Vol. 40, No. 3, 2007, pp. 605–636.

[2]Corke, T., Post, M., and Orlov, D., "Single dielectric barrier discharge plasma enhanced aerodynamics: physics, modeling and applications," *Experiments in Fluids*, Vol. 46, No. 1, 2009, pp. 1–26.

[3]Corke, T. C., Enloe, C. L., and Wilkinson, S. P., "Dielectric Barrier Discharge Plasma Actuators for Flow Control," *Annual Review of Fluid Mechanics*, Vol. 42, No. 1, 2010, pp. 505–529.

[4]Greenblatt, D. and Wygnanski, I., "The control of flow separation by periodic excitation," *Prog. Aerospace Sciences*, Vol. 36, 2000, pp. 487–545.

[5]Amitay, M. and Glezer, A., "Role of Actuation Frequency in Controlled Flow Reattachment over a Stalled Airfoil," *AIAA*

Journal, Vol. 40, 2002, pp. 209–216.

[6]Seifert, A., Greenblatt, D., and Wygnanski, I., "Active separation control: on overview of Reynolds and mach numbers effects," *Aerospace Science and Technology*, Vol. 2004, 8, pp. 569–582.

[7]Sosa, R., G., A., Moreau, E., and Touchard, G., "Stall control at high angle of attack with plasma sheet actuators," *Experiments in fluids*, Vol. 42, 2007, pp. 143–167.

[8]Benard, N., Jolibois, J., and E., M., "Lift and drag performances of an axisymmetric airfoil controlled by plasma actuator," *Journal of Electrostatics*, Vol. 67, 2009, pp. 133–139.

[9]Patel, M. e. a., "Scaling effects of an aerodynamic plasma actuator," *Journal of Aircraft*, Vol. 45, 2008.

[10]Benard, N., Braud, P., Jolibois, J., and Moreau, E., "Airflow reattachment along a NACA0015 airfoil by Surfaces Dielectric Barrier Discharge actuator Time resolved PIV Investigation," *4th Flow Control Conference*, Vol. 42, 2008.

[11]Wu, J., Lu, X., Denny, A., Fan, M., and Wu, J., "Post-stall flow control on an airfoil by local unsteady forcing," *J. Fluid Mech*, Vol. 371, 1998, pp. 21–58.

[12]Tian, Y., Cattafesta, L., and Mittal, R., "Adaptive control of separated flow," *44th AIAA aerospace Sciences meeting and Exhibit*, 2006.

[13]Raju, R., Mittal, R., and Cattafesta, L., "Dynamics of airfoil separation control using zero-net mass-flux forcing," *AIAA Journal*, Vol. 46, 2008.

[14]Guowei, Y., Shanwu, W., Ningyu, L., and Lixian, Z., "Control of unsteady vertical lift of an airfoil by leading-edge blowing-suction," *Acta Mechanica Sinica*, Vol. 13, 1997.

[15]Boucinha, V., Magnier, P., Leroy, A. and, W. R., Joussot, R., Dong, B., and Hong, D., "Characterization of the ionic wind induced by a sine DBD actuator used for laminar-to-turbulent transition delay," *4th Flow Control Conference*, Vol. 42, 2008.

[16]Dong, B., Bauchire, J., Pouvesle, J., Magnier, P., and Hong, D., "Experimental study of a DBD surface discharge for the active flow control of subsonic airflow," *Journal of Physics D: Applied Physics*, Vol. 41, 2008.